International Journal of Nanomedicine

Dovepress
Taylor & Francis Group

Open Access Full Text Article

ORIGINAL RESEARCH

The Effects of Novel Thymoquinone-Loaded Nanovesicles as a Promising Avenue to Modulate Autism Associated Dysregulation by Restoring Oxidative Stress in Autism in Mice

Nermin Eissa[1,*], Jana K Alwattar[2,*], Petrilla Jayaprakash[3], Dana Chkier[1], Aala Osama Ahmed[1], Anum Ahmed[1], Rameen Rizwan[1], Sulthan Mujeeb[1], Mohamad Rahal[2], Bassem Sadek[3]

[1]Department of Biomedical Sciences, College of Health Sciences, Abu Dhabi University, Abu Dhabi, United Arab Emirates; [2]Department of Pharmaceutical Sciences, School of Pharmacy, Lebanese International University, Beirut, Lebanon; [3]Department of Pharmacology & Therapeutics, College of Medicine and Health Sciences, United Arab Emirates University, Al Ain, United Arab Emirates

*These authors contributed equally to this work

Correspondence: Bassem Sadek, Department of Pharmacology and Therapeutics, College of Medicine & Health Sciences, United Arab Emirates University, P.O. Box 15551, Al Ain, United Arab Emirates, Tel + 971 3 7137 512, Fax + 971 3 7672 033, Email bassem.sadek@uaeu.ac.ae

Introduction: Representing a prominent public health challenge with a surge in cases and no currently available treatment, autism spectrum disorder (ASD) remains a puzzle to researchers. Although the exact pathogenesis of this heterogeneous disorder is yet to be established, it has been reported that neural oxidative stress and neuroinflammation are eminently implicated. With numerous research establishing thymoquinone (TQ) as a potent antioxidant, this study assessed its effectiveness in the context of cognitive and social impairments and neural oxidative stress in the idiopathic autistic model in BTBR mice. Moreover, a novel TQ-loaded nanovesicle drug delivery system was optimized and utilized to enhance the bioavailability of TQ in the central nervous system.

Methods: Through a battery of standard behavioral tests, primary parameters such as social behavior, locomotor activity, and anxiety levels were assessed following systemic administration with TQ (10mg/kg, i.p). Biochemical analysis of neural oxidative stress markers in the cerebellum and hippocampus tissue samples obtained from the different treatment groups was also performed.

Results: The results indicated significant enhancements in sociability and social novelty preference of assessed BTBR mice treated with TQ-loaded nanovesicles (both $p<0.01$) as well as free TQ ($p<0.05$ and $p<0.01$, respectively). Moreover, BTBR mice treated with TQ-loaded nanovesicles also displayed restored levels of anxiety ($p<0.05$) and modulated hyperactivity parameters ($p<0.05$). In addition, and following biochemical assessments, our observations revealed marked alleviation of neural oxidative stress in BTBR mice treated with TQ-loaded nanovesicles, with restored levels of antioxidant proteins, reduced glutathione ($p<0.01$), and catalase ($p<0.01$), and diminished levels of the oxidative stress byproduct, malondialdehyde ($p<0.01$).

Discussion: These preclinical observations unraveled compelling findings that reinforced TQ's antioxidant capacity, shedding new light on its potential as an effective therapeutic option for ASD. Thus, and with further experimentation, this study holds the potential to transition into a clinical study.

Keywords: autism spectrum disorder, social deficits, anxiety, hyperactivity, thymoquinone nanoparticles, BTBR mice

Introduction

Autism spectrum disorder (ASD) is a complex heterogeneous neurodevelopmental disorder that primarily influences cognitive-communication, social interaction, and behavioral patterns. It is predominantly characterized by two core symptoms presenting as social communication impairment and stereotyped repetitive and restricted patterns of behavior and interests, with marked perturbations in prefrontal, cerebellar, hippocampal, striatal, and midbrain region circuits.[1,2] The clinical core symptoms of ASD may expand to encompass speech impairment and other comorbidities.[3] The DSM-5, published by the

Received: 28 November 2024
Accepted: 23 April 2025
Published: 24 June 2025

American Psychiatric Association, outlines the criteria for diagnosing ASD. It highlights that individuals with ASD often show deficits in various areas, including cognition, sensory processing, social and emotional interactions, communication (both verbal and non-verbal), adaptive skills, executive function, and speech development, among other domains.[3,4] Some of these signs may be identified in children as young as 18 months, with an average age of diagnosis ranging from 38 to 120 months.[5] Beyond the core symptoms of ASD, individuals may also experience a range of comorbid neurological and physiological conditions, including intellectual disability, epilepsy, Attention Deficit Hyperactivity Disorder (ADHD), schizophrenia, anxiety, depression, sleep disturbances, gastrointestinal issues, and immune system dysfunction.[3,6,7] Autistic individuals often exhibit secondary symptoms such as hyperactivity, impulsivity, and aggression. They generally experience a lower quality of life, have a higher likelihood of developing comorbidities like obesity, and face an increased risk of mortality compared to the general population.[8] Early detection and intervention in managing ASD have been linked to reduced intellectual, behavioral, and functional challenges, with studies showing improvements in adaptive and motor functioning. This, in turn, lessens the overall burden on individuals with ASD and their families.[9]

Despite extensive research, there is no cure or standard treatment that fully alleviates ASD's core symptoms, likely due to its complex and heterogeneous pathophysiology. Unlike other disorders that rely on pharmacological treatments, behavioral therapy remains the only effective option for improving cognitive and speech skills in individuals with ASD.[10] There is a critical need for novel interdisciplinary studies to uncover new pathways linked to ASD development, which could lead to identifying therapeutic targets and alleviating or reversing core symptoms.

Recent research has shown that children with ASD have reduced plasma and intracellular levels of glutathione (GSH), which are linked to increased oxidative stress and damage to biomolecules like proteins and DNA. This reduction in GSH correlates with the severity of autism symptoms. As GSH levels decline in the blood and central nervous system of autistic children, oxidative stress increases, leading to DNA damage and alterations in gene expression, further contributing to neurobehavioral dysregulation.[11,12] This indicates that oxidative stress is not just a symptom of ASD but also plays a role in its development. Research suggests that oxidative stress can lead to mitochondrial dysfunction, a common issue in individuals with ASD. Therefore, targeting neural oxidative stress and related biomarkers in ASD models, such as autistic mice, should be a focus for further exploration.[13] This revelation opened doors for the promising potential of targeting oxidative stress in ASD using potent antioxidant drugs.

Medicinal plants and their active compounds are increasingly researched for their therapeutic potential, with many phytochemicals showing anti-inflammatory, anti-cancer, and cardioprotective properties. *Nigella sativa*, particularly popular in the Arab world, is recognized for its extensive health benefits and has been traditionally used to treat various diseases.[14] Thymoquinone (TQ) is noted for its strong anti-inflammatory and antioxidant properties, and it has been used to treat cognitive impairment and protect the brain from oxidative stress. Its low molecular weight and lipophilicity allow it to cross the blood–brain barrier (BBB), making it a promising therapeutic agent for neurobehavioral disorders.[15] TQ is recognized for its antioxidant, analgesic, and anti-inflammatory properties, showing effectiveness in treating liver damage, diabetes, neurodegenerative diseases like Parkinson's disease, inflammatory conditions, and various cancers. It protects cells by scavenging free radicals, chelating metal ions, enhancing antioxidant enzyme activity, and strengthening the immune system, making it a promising treatment for neurodegeneration.[16] Results of TQ treatment in Alzheimer's and Parkinson's diseases revealed that it can improve the factors leading to neurodegeneration suggesting its neuroprotective properties.[17] Based on literature analysis and review of animal data from experimental studies, it was shown that TQ exerts a significant therapeutic potential associated with its antioxidant and anti-inflammatory properties. Also, the antioxidant effect of TQ on various neurodegeneration animal models was explored. Studies have shown that TQ restores antioxidant capacity by stimulating the expression of Nrf2, a key regulator of antioxidant defenses in the brain. This reduces reactive oxygen species (ROS) formation and protects neurons from damage and loss. In animal models with elevated free radicals, GSH depletion, increased malondialdehyde (MDA), and cell death, pretreatment with TQ restored antioxidant enzymes and GSH levels while inhibiting lipid peroxidation.[18]

TQ is characterized by high lipophilicity, low bioavailability, and susceptibility to degradation under light and heat, posing significant challenges for its formulation in oral dosage forms and limiting its pharmaceutical development. Recently, various strategies have been explored to enhance its bioavailability by optimizing its physicochemical properties.[19] To enhance the bioavailability and therapeutic efficacy of TQ, nanovesicle-based drug delivery systems offer a promising approach by

improving solubility, stability, and targeted delivery. These systems enhance drug delivery and may be applied in treating ASD. However, effectively treating neurological disorders is challenging because 95% of drugs fail to cross the BBB, limiting their therapeutic impact.[20] Nanovesicles, on the other hand, have revolutionized the field of pharmaceutical research with numerous applications in treating various diseases, including neurological diseases, with high effectiveness. Hexosomes, and other internally self-assembled particles, possess unique structures and properties that facilitate the encapsulation and delivery of drugs directly to targeted sites.[21] A hexosome is a nonlamellar liquid crystalline (LC) nanoparticle with a small size, generally 95 to 105 nm, and hydrophobic characteristics that allow it to penetrate the BBB and thereby enhance the bioavailability of the pharmaceutical drug.[22] Moreover, because they degrade naturally, they are thought to be non-toxic and versatile, with the ability to be altered to ensure optimal targeted delivery.[23]

The current study hypothesized that TQ, with its antioxidant and anti-inflammatory properties, could protect the brain from oxidative damage and potentially alleviate or prevent core symptoms of ASD. To overcome the limitations of TQ's bioavailability, a novel TQ-loaded nanovesicle drug delivery system was developed, leveraging the advantages of hexosomes in the inverse hexagonal phase (H2). The study aimed to evaluate the effects of these TQ-loaded nanovesicles on cognitive deficits, social impairment, and neural oxidative stress in the BTBR mouse model, an idiopathic model of ASD. Behavioral tests like the three-chamber social assay and open field test were used to assess sociability, social novelty, locomotion, and anxiety levels. Additionally, neural oxidative stress markers, including GSH, MDA, and catalase (CAT), were measured in the cerebellum and hippocampus of treated BTBR mice.

Materials and Methods

Animals

Male BTBR mice served as the autistic mice and gender, weight, and age-matched C57/BJ6 wild-type (WT) mice served as the control; the experimental procedure was initiated on mice aged 8 to 12 weeks old. These mice were available at the animal facility of the College of Medicine and Health at UAEU, where they were bred for several generations upon originally obtaining them from The Jackson Laboratory located in Bar Harbor, Maine in the United States of America. The experimental mice were kept in well-maintained plastic cages under a standard light-dark cycle, or a 12-hour cycle, with the lights switched on at 6:00 a.m. and switched off at 5:00 p.m. The mice were housed in a specific pathogen-free and sterile environment at 22 ±2°C and were provided with standard rodent chow and water ad libitum. Trained and highly experienced laboratory staff monitored the mice's health daily with adherence to all the animal protocols approved by the Animal Care and Use Committee in the College of Medicine and Health Sciences/UAEU (Approval No. ERA-2017-5603). Oxidative stress markers were examined in the same animals that completed behavioural testing to reduce the total number of animals involved.

Formulation and Characterization of Drugs

Preparation of TQ-Loaded Hexosomal Nanovesicles

Glyceryl monooleate (GMO) was a generous gift from Gattefosse Co. (St. Priest, France), Oleic acid (OA) and Poloxamer 407 (PLX) was purchased from Sigma Co. (Sigma–Aldrich, Steinheim, Switzerland). TQ-loaded hexosomal nanovesicles were prepared using the emulsification techniques as reported by Bakr et al, through utilizing GMO and OA as the lipid phase in the presence of PLX as a stabilizer. In brief, a calculated amount of lipidic phase was mixed with PLX and heated using a thermostatically controlled water bath at 70±2°C. To this mixture thymoquinone (100mg/mL) was added and solubilized until a clear solution is obtained. The formed system was then added dropwise to a preheated aqueous solution at 70±2°C. The mixture was then emulsified using high-speed rotor-stator homogenizer (D1000, homogenizer, Benchmark Scientific Inc., NJ, USA) at 10000 rpm for 5 minutes. The prepared formulations were stored at room temperature for subsequent characterization.[24]

Experimental Design

The optimization of the hexosomal nanovesicles was conducted through factorial design methodology via examining the contributing factors and analyzing the distinguished responses affected to obtain valid objectives and reliable data.[25] In the present study, a three-factorial, two-level full factorial experimental design compromising a total of eight runs was

employed. The contributing factors' implications on the TQ loaded hexosomal nanovesicles were the concentration of GMO, OA, and PLX, and the independent variables assessed were the percentage of entrapment efficiency, particle size, and zeta potential, as elaborated in Table 1. The statistical design was constructed through Design-Expert (Design-Expert v23.1, State-Ease Inc., Minneapolis, USA).[26]

Particle Size, Polydispersity Index (PDI) Determination, and Zeta Potential Measurement

The particle size, size distribution, and zeta potential of the formed TQ-loaded hexosomal nanovesicles were determined by employing Zeta Sizer 2000 (Malvern Instruments, UK). The TQ-loaded hexosomal nanovesicles were diluted using MilliQ water and sonicated before measurements to improve measurement accuracy. All determinations were performed in triplicate.[27]

Determination of Entrapment Efficiency of TQ in Nanovesicles

To determine the entrapment efficiency of TQ loaded into the nanovesicles, free unloaded TQ whereby separated from the formulation by utilizing Vivaspin 500 centrifugal concentrator tubes with a Mwt cut of 10 kDa. The amount of TQ in the recovery chamber was quantified through high-pressure liquid chromatography (HPLC) after centrifugation at 4 ± 0.5 °C and 5000 rpm.[28] Entrapment efficiency was evaluated as follows

$$\%EE = \text{Total weight of TQ added} - \text{weight of unentrapped TQ}/\text{total weight of TQ} * 100$$

Morphological Evaluation

The structural morphology of the optimized loaded hexosomal nanovesicles was examined using transmission electron microscopy (TEM) (JEM-100 CX, JEOL, Japan). A drop of diluted dispersion was sonicated and then added to copper coated grid forming a thin film. Moreover, the thin film samples were stained using phosphotungstic acid solution (2% w/v, pH 6.8) and air-dried.[29]

In vitro Dissolution Release Studies

The in vitro release profile of TQ-loaded hexosomal nanovesicles was determined utilizing dialysis cellulose membrane bags (MWCO 12 KDa; SigmaAldrich) dipped in a dissolution apparatus filled with 750 mL phosphate buffer (pH 7.4, 37°C ± 0.5°C). At predetermined time intervals, 2 mL aliquot was withdrawn for analysis and compensated with an equivalent volume of fresh phosphate buffer over the tested period. The samples were analyzed using HPLC at λmax =254 nm.[29]

System of Analysis for TQ Determination

TQ was quantified using a validated reverse-phase High Performance Liquid Chromatography (HPLC) method, the same protocol utilized by Fakhoury et al.[30,31]

Table 1 Independent Factors and Their Respective Levels Utilized for Designing a 3^2 Full Factorial Experiment

	Low (−1)	High[1]
Independent variables		
X1= GMO %w/w	6	12
X2 = Oleic acid %w/w	0.5	1.5
X3= Poloxamer 407%w/w	2.5	5
Dependent variables		
Y1= Entrapment efficiency (%)	Maximize	
Y2= Particle size (nm)	Minimize	
Y3= Zeta Potential (mV)	Maximize	

Storage Stability Evaluation

The stability of TQ-loaded hexosomal nanovesicles for three months was evaluated through their physicochemical characteristics. Freshly prepared, optimized TQ-loaded hexosomal formulation was positioned in a glass vial and kept at room temperature for three months (25 ± 2 °C). The physical stability was assessed by evaluating the particle size, percentage entrapment efficiency, and zeta potential.[32]

Drug Administration

This study incorporated the usage of three different drugs, including the TQ-loaded nanovesicles, carrier or unloaded nanovesicles, and free TQ. To prepare for drug administration, the optimal and non-toxic dose of TQ for mice was selected based on previously published data and was determined to be 10 mg/kg[33–35.] Considering the lipophilic nature of TQ, it was necessary to utilize a solvent in which TQ was dissolved for efficacious and safe administration into the mice. Following the protocol employed by an in-vivo study where TQ was administered intraperitoneally, TQ was suspended in 0.8% Tween 80,[36] and vortexed vigorously until the suspension appeared clear. The drug compounds were freshly prepared by dissolution and vigorous vortexing before administration, and 0.1 mL/10g of body weight were administered intraperitoneally. To investigate the effects of novel TQ-loaded nanovesicles and compare their efficacy to free TQ, the experimental mice were divided into 5 distinct treatment groups, each consisting of 6 to 7 mice, and were prepared to receive chronic systemic administrations of the following solutions: 1) the C57 (WT control) and BTBR groups received 0.1 mL/10g body weight of the vehicle solution (constituting 0.9% NaCl and 0.8% Tween 80), 2) one BTBR group received 10 mg of TQ-loaded nanovesicles/kg, 3) one BTBR group received 10 mg of unloaded nanovesicles/kg and 4) one BTBR group received 10 mg of free TQ/kg (Table 2). The volume of drugs administered to each animal was 10 mL/kg, adjusted to their body weight. The drugs were administered intraperitoneally for 21 days and were administered 30 minutes before the start of each behavioral test. The schematic diagram of the study design is illustrated in Figure 1.

Behavioral Tests

On the 7th day of chronic injections, behavioral tests were initiated in which the respective drugs were administered 30 minutes prior to the test. A battery of behavioral tests was performed to assess social behavior, locomotor activity, and anxiety levels.

Three-Chamber Social Preference Assay

The first behavioral test conducted was the three-chamber social assay. This test was conducted in a transparent rectangular three-chambered polycarbonate cage, constituting a center chamber and two side chambers separated by sliding doors, with each chamber being 40 cm × 20 cm × 22 cm. There were inverted empty plastic cups placed on either side. This test assessed the preference displayed by the test mouse to explore a social stimulus (S) versus a non-social stimulus (NS), employing the 3-phase S-NS protocol.[37] The first session was the habituation session, where the test mouse was allowed to habituate for 5 minutes in the center chamber with the two side doors closed and for another 5 minutes with the doors opened to enable the test mouse to wander around and explore all three chambers. After 10 minutes of habituation, a novel mouse similar in age, gender, and weight to the test mouse, with no previous contact, was introduced under one of the cups. The choice of a cup was

Table 2 Different Treatment Groups and Respective Administered Drugs

Mouse Strain	Administered Drug
C57 Mice	Vehicle Solution (0.8% Tween 80)
BTBR Mice	Vehicle Solution (0.8% Tween 80)
BTBR Mice	TQ-Loaded Nanovesicles
BTBR Mice	Unloaded Nanovesicles
BTBR Mice	Free TQ

https://doi.org/10.2147/IJN.S509158

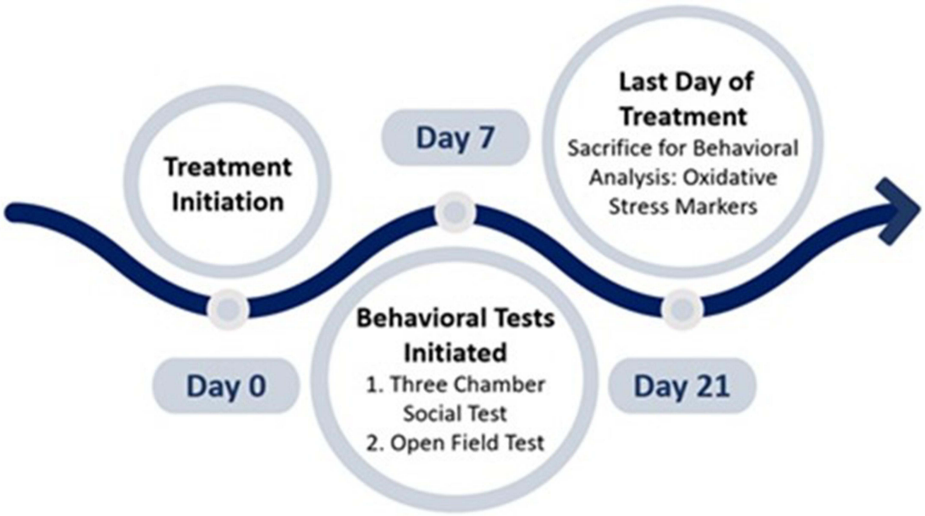

Figure 1 Schematic diagram of study design. On day 7 of treatment, behavioral tests were initiated and on day 21 of treatment, the mice were sacrificed for biochemical analysis.

random to avoid side preference. The introduced mouse was referred to as the novel mouse and the empty cup was referred to as the novel object. The novel mouse represented 'S' while the empty cup in the other chamber served as a 'NS'. The test mouse was allowed to explore for 10 minutes, and the exploration time was recorded. This phase of the three-chamber test assessed sociability parameters by analyzing the mouse's interactions with social and non-social stimuli.[38] The next phase of the test assessed social novelty preference. A second novel mouse of similar age, gender, and weight to the test mouse was placed under the empty cup and was referred to as the novel mouse while the mouse from the previous phase was now referred to as the familiar mouse. The experimental mouse allowed to explore the chambers for 10 more minutes, and the exploration time was recorded. This phase examined the mouse's preference to explore the 'unfamiliar social stimulus' over the 'familiar social stimuli.

The total time for the three-chamber test was 30 minutes for each test mouse. A camera was placed above the chambers, which automatically recorded the time that the test mouse spent with the empty cup, the novel mouse, and the familiar mouse. The Noldus EthoVision software automatically scored and recorded the time spent in each chamber for the three phases. Additionally, the chambers, doors, and cups were cleaned with 70% ethanol after each experiment to avoid the current experimental mouse from recognizing the scent of the previous experimental mouse.[38] A direct comparison of the social behavior of the different treatment groups was made by calculating the sociability index (SI) and social novelty index (SNI) using the following equations 2 and 3, respectively.

$$Sociability\,Index = \frac{(time\ spent\ with\ novel\ mouse - time\ spent\ with\ novel\ object)}{(time\ spent\ with\ novel\ mouse + time\ spent\ with\ novel\ object)}$$

Equation 1. Sociability index is calculated by subtracting the time spent with the novel object from the time spent with the novel mouse and dividing this number by the total time spent with the novel mouse and novel object.

$$Social\ Novelty\ Index = \frac{(time\ spent\ with\ novel\ mouse - time\ spent\ with\ familiarmouse)}{(time\ spent\ with\ novel\ mouse + time\ spent\ with\ familiar\ mouse)}$$

Equation 2. Social novelty index is calculated by subtracting the time spent with the familiar mouse from the time spent with the novel mouse and dividing this number by the total time spent with the novel mouse and familiar mouse.

Upon calculating SI and SNI, the average and standard error mean values of these measurements were calculated as well using Microsoft Excel. The results were represented as bar graphs.

Open Field Test

The second behavioral test that was conducted was the open-field test (Figure 2), which systematically assessed the exploratory activity exhibited in a novel open-field environment. This test serves as an independent control for the effects of the drugs on physical activity that may confound the interpretation of any self-grooming, anxiety levels, or spontaneous alteration results. This test was conducted in a square-shaped cage ranging 45 × 45 × 30 cm and providing an open-field arena for the mouse to explore and wander around, with the center region defined as the central 23 × 23 cm area. The test mouse initially allowed 5 minutes of habituation. After habituation, 10 minutes were provided for the mouse to explore freely. The total time for the open field was 15 minutes for each test mouse. The chamber was thoroughly cleaned with 70% ethanol and allowed to dry before the start of a new test. This test assessed locomotor activity by measuring the total distance traveled by the mouse in the whole arena, and anxiety levels by measuring and comparing the total time spent in the center to the time spent in the periphery of the chamber [69]. Similar to the three-chamber social test, a camera was placed above the chamber to record the measurements. The average and standard error mean values of the total distance traveled (cm), time spent in the center (s), and time spent in the periphery (s) were calculated.

Biochemical Assessments

Upon 21 days of chronic treatment, the mice were sacrificed, and their brain tissue samples were collected and homogenized for biochemical analysis of neural oxidative stress markers.

Sacrifice and Brain Tissue Sample Collection

Each group was injected with its respective drug 30 minutes before the administration of anesthesia. Once 30 minutes had passed, the mouse was intraperitoneally injected with 0.4 mL of pentobarbital and kept in a separate cage where it fell asleep. It was required to wait 3 to 4 minutes after injecting pentobarbital for deep anesthesia to be achieved. Once the mouse was asleep, it was pinned by the limbs onto a Styrofoam board to undergo cardiac perfusion. A cut across the abdomen was made to expose the heart and internal organs. This step was done very carefully to avoid any damage to the organs of the mouse. Once the heart of the mouse was easily accessible, an incision was made on the right atrium of the heart, which was visualized as the darkest part of the heart. This incision allowed the phosphate-buffered saline (PBS) to flow out during perfusion. The purpose of cardiac perfusion is to wash out the blood from the brain, so it does not interfere with biochemical analysis. A syringe filled with PBS (1X, pH 7.4) was injected at the bottom of the heart to wash out the blood from the organs. The Styrofoam board was placed on top of a water-filled tub that collected the blood and PBS. Cardiac perfusion was performed until the liver had turned a lighter pinkish shade. The head was then decapitated, and the brain was quickly extracted and placed on an ice plate, where it was dissected into several parts, including the cerebellum, hippocampus, striatum, prefrontal cortex, and cortex. The different brain parts were placed in labeled tubes and flash-frozen in liquid nitrogen. Once all the brain samples were extracted, the tubes were arranged in labeled boxes and stored at –80°C until homogenization.

Figure 2 Open field test setup. The center and peripheral regions of the chamber are highlighted.

https://doi.org/10.2147/IJN.S509158

Tissue Preparation for Biochemical Analysis

For biochemical analysis, cerebellum and hippocampus brain tissue samples were used. The first step was to homogenize the cerebellum and hippocampus tissue samples. For homogenization, the samples had to be thawed on ice for about 15 to 20 minutes before homogenization. The weight of each sample was determined, and an appropriate volume of RIPA buffer and protease phosphatase inhibitor cocktail was added to preserve the proteins in the samples. In another set of tubes, different-sized beads were added to facilitate homogenization. For cerebellum tissue samples, 4 big and 5 small beads were added, while only 5 small beads were needed for hippocampus tissue samples. Once all of this was done, the RIPA buffer was added to each tube. The amount of RIPA buffer to be added was calculated using Equation 3.

$$Amount\ of\ RIPA\ buffer\ =\ weight\ of\ brain\ tissue \times 10$$

Equation 3. The amount of RIPA buffer to be added is calculated by multiplying the weight of the brain tissue sample by 10.

The brain tissue samples were added to the bead-filled tubes and then homogenized at 14,000 rpm for 30 minutes at 4°C to eliminate tissue debris. Once homogenized, the solution was transferred to a clean, new tube, which was then centrifuged at 10,000× for 30 minutes at 4°C. Once centrifuged, the supernatant was decanted into its original tube, and the samples were ready to use.

Neural Oxidative Stress Levels Assessment

Neural oxidative stress markers in the cerebellum and hippocampus tissue samples were assessed. Each biomarker had its kit with its own set of instructions to follow. The biomarkers tested were CAT, MDA, and GSH. CAT represented a prominent antioxidant enzyme, GSH represented a vital antioxidant protein, and MDA represented a major lipid peroxidation, or oxidative stress, byproduct.

Evaluation of Catalase Levels

The protocols of the Catalase Assay Kit provided by Cayman Chemical (MI, USA) (item number 707002) were followed. The Nunc 96-well microplates from Thermo Fisher Scientific (catalog number 243656) were utilized. In brief, formaldehyde standard wells were prepared using 100 µL of CAT assay buffer, 30 µL of methanol, and 20 µL of the formaldehyde standard. The same amounts of buffer and methanol were added for the positive control wells, along with 20 µL of diluted CAT. The samples were diluted using the CAT sample buffer. The sample wells were prepared similarly, with the addition of the diluted sample. The reactions were initiated by quickly adding 20 µL of diluted hydrogen peroxide to all wells, noting the precise reaction initiation time. The plate was covered and incubated using the thermoshaker PST-60HL by Biosan (MI, USA) for 20 minutes at room temperature. The reactions were terminated upon the addition of 30 µL of potassium hydroxide, followed by 30 µL of Catalase Purpald (the chromogen) to each well. The plate was again covered and incubated for 10 minutes at room temperature. Finally, 10 µL of catalase potassium periodate was added, and the plate was covered and incubated for another 5 minutes at room temperature. The absorbance was read at 540 nm using the plate reader Infinite M200 Pro and the software i-control I.II by Tecan Life Sciences (Männedorf, Switzerland) with results expressed in CAT concentration (µM).

Evaluation of Malondialdehyde Levels

The protocols of the Malondialdehyde Assay Kit provided by Northwest Life Science Specialties (Vancouver, WA, USA) (product NWK-MDA01) were followed. In brief, 10 µL of butylated hydroxytoluene was added to a microcentrifuge vial, followed by the addition of 250 µL of samples or calibrators. 250 µL of acid reagent and 250 µL of 2-thiobarbituric acid were then added, and the mixture was vortexed vigorously. The samples and calibrators were then incubated for 60 minutes at 60°C and centrifuged afterward at 10,000× for 2 to 3 minutes before being transferred to a cuvette. The absorbance was read at 532nm using the microplate reader with results expressed in MDA concentration (µM).

Evaluation of Reduced Glutathione Levels

The manufacturer's protocols of the Glutathione Assay Kit provided by Sigma-Aldrich (St. Louis, MO, USA) (catalog number CS0260) were followed. In brief, the 5,5'-dithiobis (2-nitrobenzoic acid) (DTNB) stock solution was prepared

using DTNB and dimethyl sulfoxide, and the NADPH stock solution was prepared by diluting NADPH. A series of standard solutions of different concentrations were prepared through serial dilution. This is followed by the addition of 5% 5-sulfosalicylic acid (SAS), which deproteinizes the samples. SAS was added to the samples, which were centrifuged to obtain the supernatant and remove the precipitated protein. The samples and standards were added to the wells of a 96-well microplate and incubated with the DNTB solution, assay buffer, and GSH reductase for 5 minutes at room temperature. Subsequently, the diluted NADPH solution was added and mixed thoroughly. The absorbance was measured at 412 nm using a microplate reader with results expressed in GSH concentration (μM).

Statistical Analysis

Data were expressed as the mean ± standard error of the mean. The effects of different modifications of the drug on behavioral tests and biochemical analyses in the C57 and BTBR mice groups were analyzed using a two-way analysis of variance (ANOVA). To assess the statistical significance between the different study groups, post hoc comparisons were conducted using Tukey's test. The PRISM statistics software (GraphPad Software, San Diego, CA, USA) was utilized for all statistical analyses. A significance level of $p < 0.05$ was employed to determine statistical significance.

Results

Optimization of the TQ-Loaded Hexosomal Nanovesicles: Particle Size and Polydispersity Index Analysis

The particle size of the prepared eighth TQ-loaded hexosomal formulations is present within the nanometric range, ranging between 101.3±1.11nm and 210.1±12.4nm, as demonstrated in Table 3. The PDI values for the eight formulations were less than 1, which confirmed the homogeneity and narrow (unimodal) distribution. Statistical analysis using ANOVA revealed that the linear model for evaluating the particle size using the selected variables is significant through a P value = 0.0421 and correlation coefficient (R2) of 0.952, thus signifying that 95.2% of the variation is dependent on the three variables studied. Moreover, the residual analysis and ANOVA confirmed the suitability of the model as the predicted R-squared of 0.905 agreed with the adjusted one of 0.879. For a better understanding of the analysis, surface plot curves are presented as both two-dimensional and three-dimensional, as well as the perturbation curve through Design Expert, demonstrating the strength of the variables' impact as shown in Figure 3A.

The regression equation evaluating the influence of GMO (A), OA (B), and PLX (C) concentration on particle size is represented by equation 4. From the regression equation, it was clear that GMO and OA had a positive influence on the particle size, contrary to the PLX, which presented a negative effect.

Equation 4.

$$Particlesize(nm) = +152.70000 + 21.20000A + 16.00000B - 16.47500C - 8.75000AB - 1.27500AC$$

Determination of the Zeta Potential of Thymoquinone Loaded Hexosomal Nanoparticles

The prepared TQ-loaded hexosomal nanoparticles presented high zeta potential with a negative charge, which ranged between −26.2±0.15 mV and −38.3±0.54 mV, as given in Table 3.

ANOVA analysis demonstrated the ability of the mathematical model to examine the influence of the independent variables on the zeta potential (P value <0.0407). The suggested model presented an R2 equal to 0.982, indicating that the zeta potential is significantly influenced by the independent variables, with the predicted R2 (0. 934) and adjusted R2 (0.893) in close agreement, with a difference of less than 0.2. The adequacy/precision ratio for that dependent variable exceeds 4, demonstrating the signal's capability to effectively explore the design space. Moreover, the two-dimensional and three-dimensional surface plots, along with the interaction graphs shown in Figure 3B, illustrate the influence of GMO, OA, and PLX concentrations on the zeta potential of the TQ-loaded hexosomal nanovesicles.

Table 3 Particle Size (nm), Percentage Entrapment Efficiency, and Zeta Potential (mV) of the Different Prepared Formulations of Thymoquinone-Loaded Hexosomal Nanovesicles Prepared According to 2^3 Full Factorial Designs (n=3±SD)

Formula	GMO Concentration %w/w	Oleic Acid Concentration %w/w	PLX Concentration %w/w	Particle Size (nm)	Entrapment Efficiency (%)	Zeta Potential (mV)
F1	1	−1	−1	173.2±2.89	96.2± 1.17	−28.1±0.4
F2	1	−1	1	160.1±6.37	92.3±0.47	−30.3±0.95
F3	−1	1	1	131.3±10.2	93.1±0.78	−32.1±1.55
F4	1	1	1	152.2±5.50	98.1±0.42	−38.3±0.54
F5	−1	1	−1	181.2±4.16	92.3±0.78	−31.2±1.82
F6	1	1	−1	210.1±12.4	93.1±2.1	−35.2±2.3
F7	−1	−1	−1	112.2±8.1	94.2±1.73	−26.2±0.15
F8	−1	−1	1	101.3±1.11	91.1±1.63	−30.2±1.45

The regression equation assessing the impact of GMO (A), OA (B), and PLX (C) concentration on Zeta potential is represented by Equation 5. From the equation, it was evident that all three independent variables positively impacted the zeta potential, with the oleic acid being the prominent contributor between all three as it presented the highest coefficient.

Equation 5.

$$\text{Zeta potential (mV)} = \quad + 31.45000 + 1.52500\ \text{A} + 2.75000\,\text{B} + 1.27500\,\text{C}$$

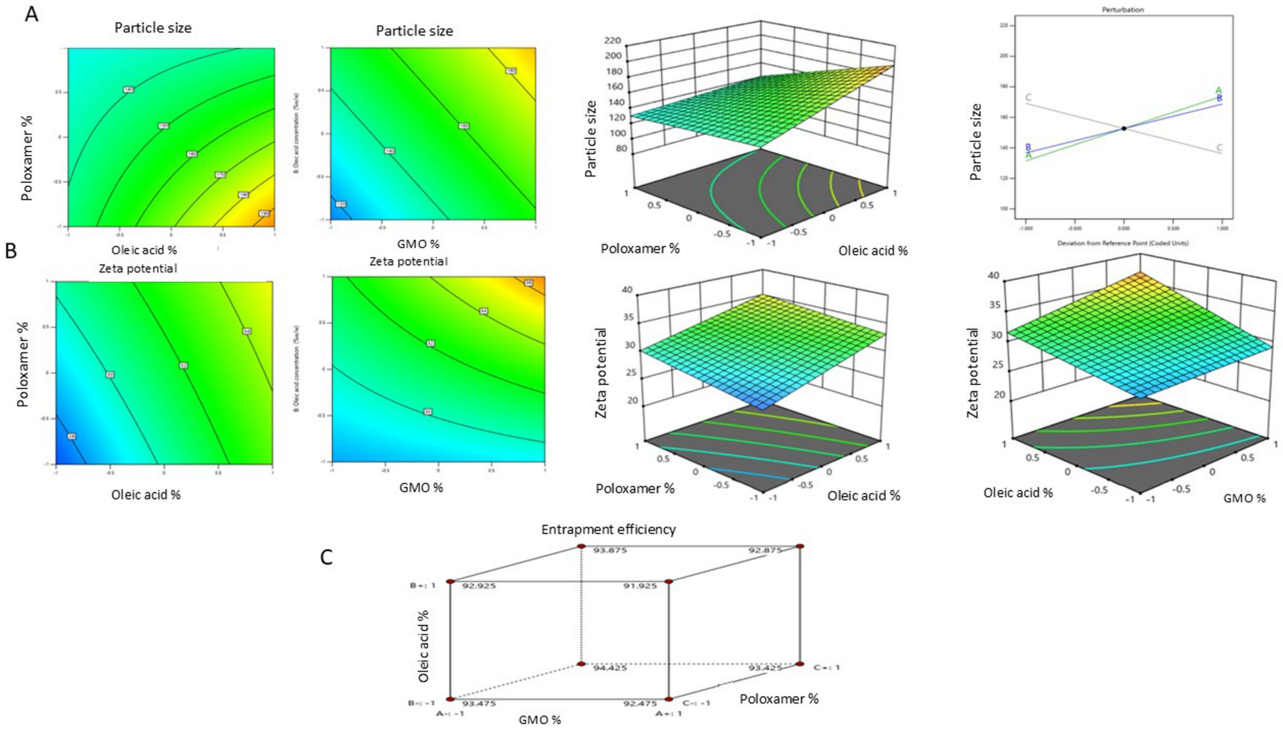

Figure 3 The multivariable impact of GMO, PLX, and OA concentrations on (**A**) the particle size of thymoquinone-loaded nanovesicles illustrated by two-dimensional, three-dimensional and perturbation plots (**B**) the zeta potential demonstrated by two-dimensional contour plots and three-dimensional contour plot and (**C**) entrapment efficiency through the Cubic graph.

Entrapment Efficiency of Thymoquinone in Hexosomal Nanovesicles

The entrapment efficiency of the eight TQ-loaded hexosomal formulations was determined to quantify the amount of TQ loaded in the nanovesicle. As illustrated in the cubic graph in Figure 3C, the EE% was influenced by variations in GMO, PLX, and OA concentrations (w/w%). The data revealed that the amount loaded in the hexosomal phase concerning the total drug quantity added during preparation revealed an encapsulation efficacy in the range of 91.1±1.63% to 98.1 ±0.42%, as demonstrated by Table 3.

Check Point Analysis

Validation of the Statistical Model

Validation of the statistical model was obtained through the close agreement of adjusted R2 and the predicted R2 for the three responses with the high R2 coefficient. Moreover, a small percentage error <10% was attained between actual/predicted response variables.[11]

Selection of the Optimal TQ-Loaded Hexosomal Nanovesicles Formulation

The optimal values of the variables were determined through numerical analysis using the program, guided by the desirability criterion. The ideal TQ-loaded hexosomal formulation was composed of 5.112 (w/w %) GMO, 0.43 (w/w %) OA, and 4.5 (w/w %) PLX. As shown in Table 4, the expected values for EE%, particle size, and Zeta potential were 95.2%, 102.4 nm, and −32.8275 mV, respectively. The optimal formula was prepared and validated, as shown in Table 4, with a relative error of less than 10% from the predicted values generated by the Design Expert software, indicating the model's accuracy.[12]

In-vitro Release Profile of TQ from Optimized Loaded Hexosomal Nanovesicle

The in vitro release profile of TQ from optimized loaded hexosomal nanovesicles exhibited a sustained release manner for 24h, as illustrated in Figure 4. It was observed that more than 17.5% of TQ was released within the first 4 h.

Morphological Evaluation of Loaded Hexosomal System

The morphology examination by TEM employed to examine the nanostructure of the drug-loaded hexosomal nanoparticles revealed a clear hexagonal structure, as presented in Figure 5.

Storage Stability of Thymoquinone-Loaded Hexosomal Nanovesicles

The optimized TQ-loaded hexosomal nanovesicles at room temperature for three-month periods were investigated through particle size, zeta potential, and % EE. Insignificant fluctuations were attained in the particle size, zeta potential, and %EE between fresh samples and 3-month stored samples, as demonstrated by Table 5.

Table 4 Composition and Validation of the Optimum Thymoquinone-Loaded Hexosomal Nanovesicles with Their Expected Responses

The Optimized Formula	**Formulation variables**			**Dependent Responses**		
	GMO Concentration w/w %	**Oleic Acid Concentration w/w %**	**PLX Concentration w/w %**	**Entrapment Efficiency %**	**Particle Size (nm)**	**Zeta Potential (mV)**
	5.11	**0.45**	**4.5**	**95.2**	**102.4**	**−32.8275**
Validation of the optimum formula						
Responses	Predicted value	Experimental value		% Relative error		
EE%	95.2	94.3		1.166		
Particle size	102.4	108.3		5.76		
Zeta potential	−32.8275	−31.32		4.5907		

https://doi.org/10.2147/IJN.S509158

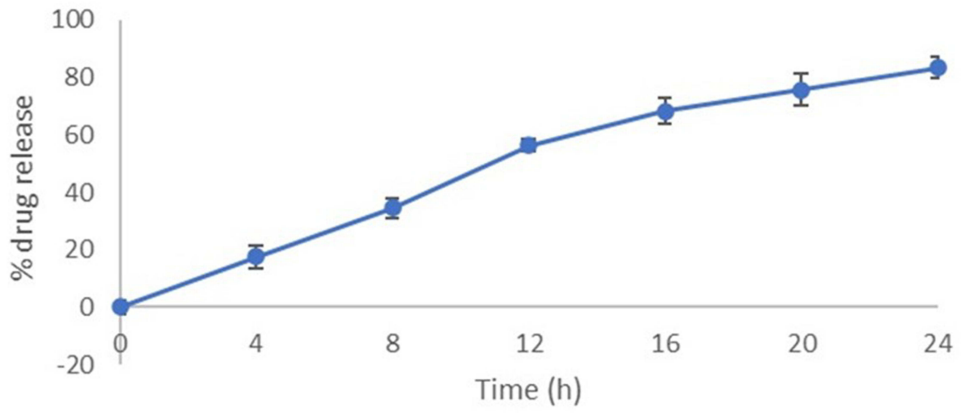

Figure 4 In vitro release profile of optimized thymoquinone loaded hexosomal nanovesicles with in phosphate buffer (pH 7.4, 37° C ± 0.5° C).

Effects of TQ Treatments on Sociability and Social Novelty Preference in BTBR Mice

Heatmaps obtained from the trials of C57 and BTBR mice were analyzed to compare the typical behaviors observed in the normal C57 mice and autistic BTBR mice. Figure 6A and B represent heatmaps that demonstrate the overall social behavior exhibited by the C57 control mice and BTBR autistic mice during the three-chamber social test, respectively. It was evident that the C57 mouse spent more time exploring the novel mouse over the empty cup during the sociability assessment session (Trial 13 in Figure 6A) and more time exploring the novel mouse over the familiar mouse during the social novelty preference assessment session (Trial 14 in Figure 6A). On the other hand, while it appeared that the BTBR mouse spent time exploring the novel mouse (Trial 11 in Figure 6B), it showed no preference towards the novel mouse in the third session of the test (Trial 12 in Figure 6B). To evaluate the effects of the TQ-loaded nanovesicles in the context of social communication, specifically in terms of sociability and social novelty preference, the three-chamber social assay was conducted. Statistical analysis of the results, which included a two-way ANOVA and Tukey's post-hoc test, was then performed to assess statistical significance.

The SI values are displayed in Figure 7A. The mice from the BTBR vehicle group exhibited notable sociability impairment represented by a low SI ($F(1,8) = 12.41$, $p<0.05$) compared to the control mice from the C57 vehicle group. Remarkable improvement in sociability was evident in mice from the empty nanovesicle carrier, TQ-loaded nanovesicles, and free TQ groups with significant enhancement upon treatment with TQ-loaded nanovesicles ($F(1,8) = 14.58$, $p<0.01$)

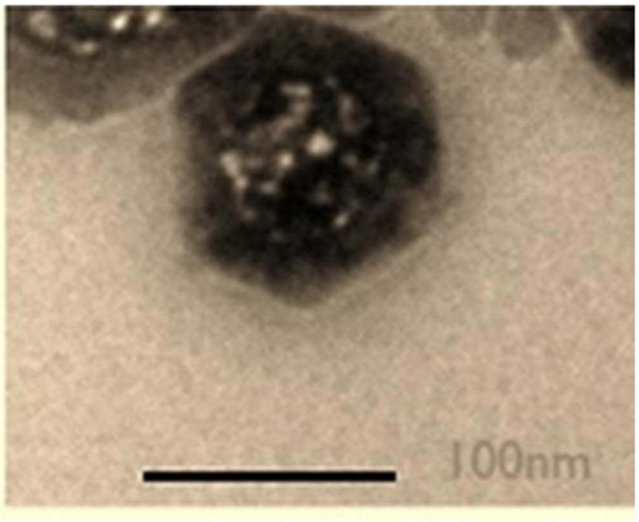

Figure 5 Transmission electron photomicrograph of the optimized thymoquinone-loaded hexosomal nanovesicles.

Table 5 Effect of Three-month Storage at Room Temperature on the %EE, Particle Size, and Zeta Potential of the Optimized Formulation

Responses	Fresh	After 3 Months
EE%	94.3± 0.48	93.1 ± 3.51
Particle size	108.3± 5.2	110.02 ± 6.3
Zeta potential	−31.32± 1.27	−32.14 ± 2.3

and free TQ ($F(1,8)= 7.63$, $p<0.05$). Among the TQ-loaded nanovesicles and free TQ treatment groups, treatment with TQ-loaded nanovesicles gave a more significant result ($F(1,7)=5.22$, $p<0.05$), indicating that the delivery of TQ within the nanovesicles instigates substantial enhancement in the sociability exhibited by the BTBR mice.

The SNI was also calculated and analyzed (Figure 7B). The mice from the BTBR vehicle group displayed profoundly impaired social novelty preference ($F(1,8)=12.58$, $p<0.01$) as compared to the control mice from the C57 vehicle group. Significant enhancement of social novelty preference, reflected by an increased SNI, was observed upon treatment with TQ-loaded nanovesicles ($F(1,8)=7.63$, $p<0.05$) and free TQ ($F(1,8)=18.06$, $p<0.01$). Both groups showed similar results with the same statistical significance, while treatment with the unloaded nanovesicles did not show any improvement in social novelty preference.

Effects of TQ Treatments on Locomotor Activity and Anxiety Levels in BTBR Mice

To evaluate the effects of the TQ-loaded nanovesicles in the context of cognitive behavior, in terms of locomotor activity and anxiety levels, the open field test was conducted. Locomotor activity was assessed by measuring the total distance traveled by each mouse. This test indicates the general activity levels of mice and is typically applied when studying the effects of various treatments on the physical activity and behavioral response of the mice. As revealed in Figure 7C, a significantly longer distance was traveled by mice from the BTBR vehicle group in the chamber ($p<0.001$) when

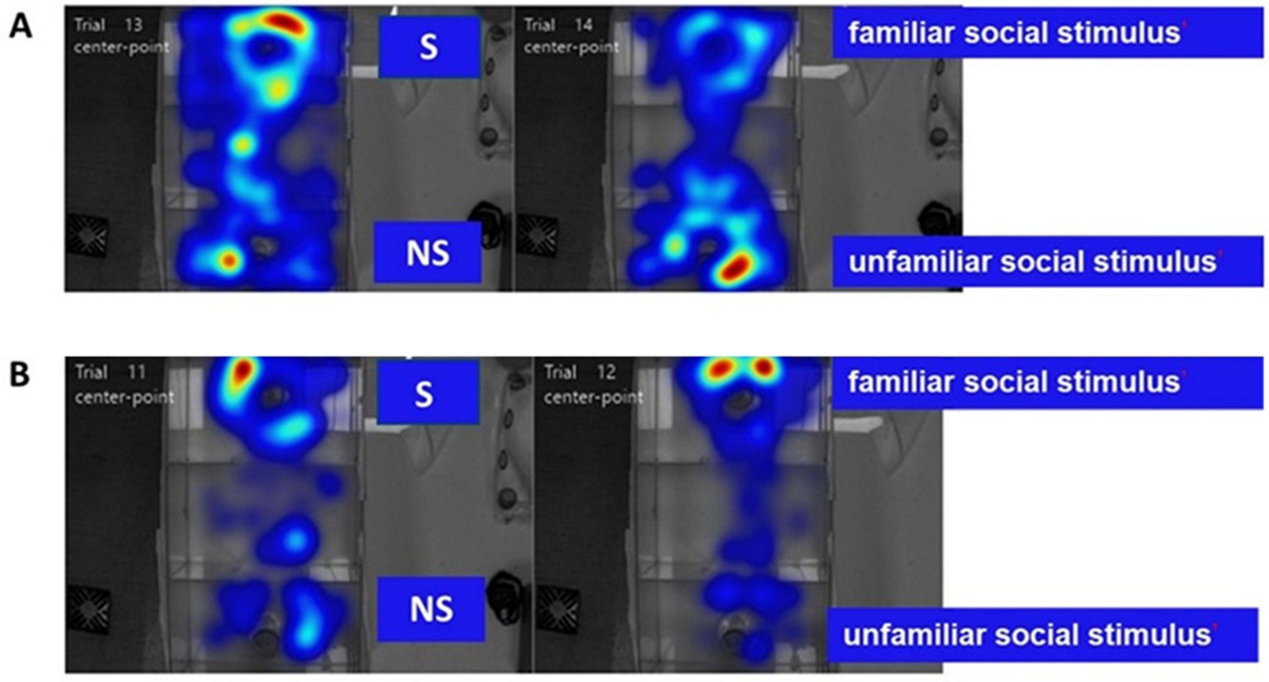

Figure 6 Behavior of C57 and BTBR mice during the three-chamber social test. (**A**) Social behavior exhibited by a C57 test mouse. (**B**) Social behavior exhibited by a BTBR test mouse.
Abbreviations: S, Social stimulus; NS, Non-social stimulus.

https://doi.org/10.2147/IJN.S509158

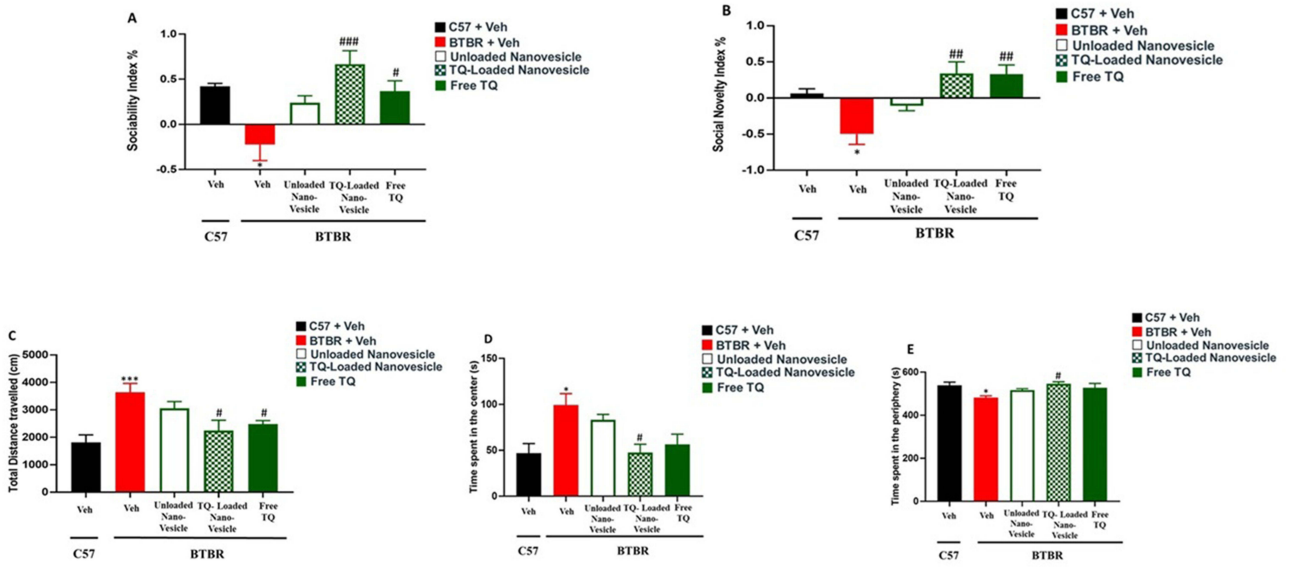

Figure 7 Behavioral test results for the different treatment groups. (**A**) Sociability index. (**B**) Social novelty index. (**C**) Total distance traveled in the chamber. (**D**) Time spent in the center of the chamber. (**E**) Time spent in the peripheral regions of the chamber. *p<0.05 BTBR Vs Veh-treated C57; ***p<0.001 BTBR Vs Veh-treated C57; $^{\#}$ p<0.05 BTBR Vs Veh-treated BTBR; $^{\#\#}$ p<0.01 BTBR Vs Veh-treated BTBR; $^{\#\#\#}$ p<0.001 BTBR Vs Veh-treated BTBR.

compared to the control mice from the C57 group, reflecting hyperactivity. Treatment with TQ-loaded nanovesicles ($F(1,10) = 7.91$, $p<0.05$) and free TQ ($F(1,10)=10.92$, $p<0.01$) modulated hyperactivity in the BTBR mice, where the mice traveled shorter distances in the chamber.

Anxiety levels were evaluated by measuring the time spent in the center (Figure 7D) compared to the time spent in the periphery of the chamber (Figure 7E). The mice from the BTBR vehicle group spent significantly more time in the center ($F(1,10)=18.63$, $p<0.01$) compared to the control mice, indicating cognitive impairment and impulsive behavior, reflecting abnormal anxiety. Treatment with TQ-loaded nanovesicles ($F(1,10)=21.55$, $p<0.01$) restored abnormal anxiety in the BTBR mice, where they spent significantly less time in the center compared to the periphery.

These results suggest that the utilization of TQ-loaded nanovesicles yields the best results in terms of sociability and social novelty preference enhancement, hyperactivity modulation, and abnormal anxiety restoration. These effects may be attributed to decreased oxidative stress in the brain, which was also investigated in this study.

Effect of TQ Treatment on Neural Oxidative Stress Markers

CAT concentration in the cerebellum and hippocampus brain tissues was determined (Figure 8A). In the cerebellum tissue samples of the BTBR vehicle group mice, there was a profound diminishment in CAT concentration as compared to the levels measured in the brains of the control mice from the C57 vehicle group. Upon treatment with TQ-loaded nanovesicles and free TQ, a significant increase in CAT levels was measured in the cerebellar tissue samples obtained from the BTBR mice. Similarly, in the hippocampus tissue samples of the BTBR vehicle group mice, there was also a decrease ($p<0.01$) in CAT concentration as compared to the concentration measured in the brains of the control mice from the C57 group. Upon treatment with both TQ-loaded nanovesicles, there was remarkable restoration and replenishment of CAT levels in the hippocampal tissue samples obtained from the BTBR mice. Overall, there was a more statistically significant decrease in CAT levels in the hippocampus of BTBR vehicle group mice as compared to the levels measured in the cerebellum. In the cerebellum, improvement in the levels of CAT was recorded in two treatment groups, the BTBR groups receiving TQ-loaded nanovesicles and free TQ treatment, whereas in the hippocampus, improvement was only identified in one treatment group, the BTBR group receiving the TQ-loaded nanovesicles treatment.

MDA concentration in the cerebellum and hippocampus was determined (Figure 8B). In the cerebellum of the BTBR vehicle group mice, there was a marked elevation of MDA levels as compared to the levels measured in the brains of the control mice from the C57 vehicle group. A significant decrease in MDA levels was observed in the BTBR mice treated

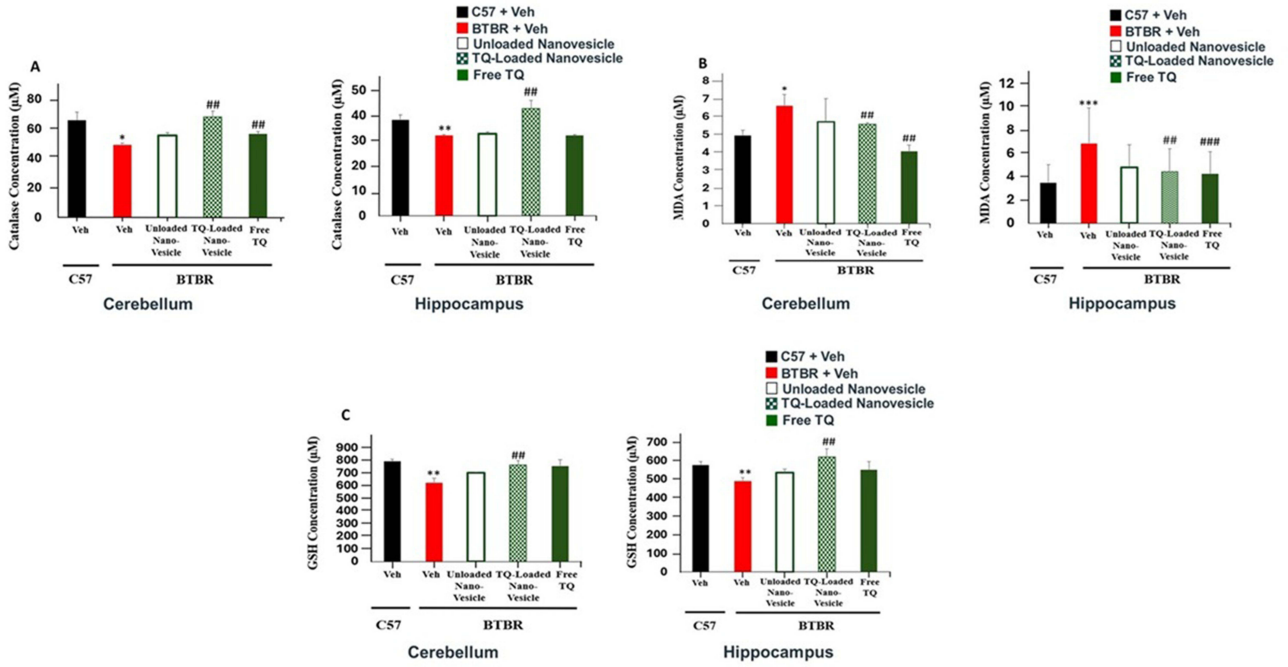

Figure 8 Biochemical analysis of neural oxidative stress in the cerebellum and hippocampus tissue samples obtained from the different treatment groups. (**A**) Catalase concentration. (**B**) Malondialdehyde concentration. (**C**) Reduced glutathione concentration. *p<0.05 BTBR Veh Vs C57 Veh; **p<0.01 BTBR Veh Vs C57 Veh; *** p<0.001 BTBR Veh Vs C57 Veh; ## p<0.01 BTBR Veh Vs BTBR treated; #### p<0.001 BTBR Veh Vs BTBR treated.

with TQ-loaded nanovesicles and free TQ. In the hippocampus of BTBR vehicle group mice, there was also an increase in MDA concentration as compared to the control mice from the C57 group; however, it was more significant than in the cerebellum. Upon treatment with both TQ-loaded nanovesicles and free TQ, there was a significant decrease ($p<0.01$ and $p<0.001$, respectively) in MDA levels. Overall, there was a more statistically significant increase in MDA levels in the hippocampus tissues of the BTBR vehicle group mice as compared to the cerebellum tissues. Diminishment in MDA levels in both the cerebellum and hippocampus tissues was observed in two treatment groups, the BTBR mice receiving TQ-loaded nanovesicles and the BTBR mice receiving free TQ. Nonetheless, free TQ induced a more significant decrease in MDA levels within the hippocampus than within the cerebellum.

GSH concentration was assessed in the cerebellar and hippocampal tissues (Figure 8C). Similar results were observed in both tissues. In the cerebellum and hippocampus tissue samples obtained from the BTBR vehicle group mice, there was a significant reduction in GSH levels compared to the levels measured in the brains of the C57 control mice. Remarkable restoration and replenishment of GSH levels in the cerebellum and hippocampus were observed in the BTBR group treated with the TQ-loaded nanovesicles.

The observed results of the assessed neural oxidative markers aligned with the improvement observed at the behavioral level suggesting the implication of oxidative stress in the social impairment observed in ASD.

Discussion

The biopharmaceutical bioavailability of TQ-loaded hexosomal nanovesicles is highly dependent on the particle size of this system, where this parameter is a determinate factor for absorption and uptake. Moreover, the PDI is a direct indicator of the system's homogeneity; whereas the value approaches zero, it indicates a more uniform dispersion.[39] The particle size of the various formulations was within the nanometric range with a narrow distribution validated by PDI of less than 1, which is similar to the previous findings by Mohammad et al.[39] In this study, ANOVA analysis revealing the P value of less than 0.05 and high correlation coefficient reflect that the changes in particle size are dependent on the variables at hand. Additionally, the predicted R-squared was in close alignment with the adjusted R-squared, suggesting that the underlying model is significant.[40] The influence of the tested variables on particle size is highlighted by various

https://doi.org/10.2147/IJN.S509158

studies, In a study by Badie et al, the positive impact of GMO on the particle size was explained by the increase in matrix viscosity upon the increase in GMO concentration, hence impeding the uniform dispersion of the water phase leading to this increase in particle size.[41–43] The same study reported that the increase in OA decreased the particle size, which was due to the hydrophobic interaction and solubilization of OA, thereby increasing the hydrocarbon chain and causing an increase in molecular packing. Contrary to these findings, Bakr et al's study reported that the increase in OA decreased particle size, which was justified by a decrease in hydrophobicity in the lipid core due to the OA negative charge.[24] Moreover, both Badie et al and Bakr et al concurred on the impact of PLX where its increase led to a significant decrease in particle size similar to our findings which was explained by the poloxamer's ability to stabilize the interface and reduce the surface tension allowing better dispersion of the water phase thus demonstrating a smaller and more uniform emulsion.[24,42]

The zeta potential of nanovesicles determines the surface properties that influence the stability of the system. High values of zeta potential of ±25 mv and above indicate a strong repulsive interaction among the formed nanovesicles, which maintains strong physical stability. This repellent activity prevents coalescence of the dispersed phase due to the high barrier activity, thereby ensuring greater colloidal stability.[44] The zeta potential of the different formed formulations was assessed by ANOVA, revealing the significant influence of the three variables through a P value = 0.0104, with the three variables presenting a positive impact on the zeta potential. In the current study, the increase in GMO concentration led to a significant increase in absolute zeta potential values, which can be attributed to the negative charges carried by the ionized carboxylic group of free OA present in the raw material. These findings were concurrent with the study of Zaki et al.[32] Similarly, the increase in OA concentration resulted in a positive effect on the zeta potential, which was driven by the same mechanism. Additionally, the addition of PLX also presented a significant positive influence on the zeta potential values, which can be explained by the presence of hydroxyl ions that react with the surrounding aqueous environment, generating a negative charge at the interface between water and lipids.[45] These results were similar to Badie et al, which attributed this phenomenon to the creation of a coating layer that ensures sufficient stabilization through steric hindrance.[42]

The encapsulation of the drug in a nanovesicle is an essential parameter for the optimal development of a drug delivery system. Achieving high entrapment efficiency facilitates effective therapeutic application, which also contributes to lowering systemic side effects. In the current study, high levels of entrapment were observed across the various formulations, this outcome is linked to the enhanced solubility of the hydrophobic drug TQ within the lipid bilayers, permitting a strong affinity and ensuring successful incorporation. This finding was in good agreement with the Swarnakar et al study reporting an entrapment efficiency of progesterone greater than 95% within the hexosomal formulation.[45] The morphological characterization of the optimized TQ-loaded hexosomal formulation was examined through TEM. The examined formulation showed monodispersed nanovesicles with six-sided outer hexagonal configuration as reported in various studies.[46] The hexagonal transformation can be attributed to the addition of OA which induces the phase transition from cubic LC structure to hexagonal LC mesophase. The OA presence acts as a lattice modifier as it increases the lipidic volume, increasing the packing parameter. In nanomedicine, achieving a sustained release profile is a critical factor for the effective development of drug delivery systems. Our release data showed the ability of TQ-loaded hexosomal nanovesicles to produce a sustained release. The retention of the drug in hexosomes indicates the complete incorporation of the drug within the lipidic bilayer, providing an outstanding prolonged release feature. Similar findings were obtained by fluoxetine release from GMO-based hexosomal nanoparticles reported by Abdel Bar et al.[47] For three-month period, the optimized TQ-loaded hexosomal nanovesicles retained their particle size, with both the zeta potential entrapment efficacy remaining consistent with measurements from fresh samples. These results confirm that the optimized TQ-loaded nanovesicles remained stable under storage conditions. These findings align with the study by Abdel Bar et al, which reported that fluoxetine hexosomal formulation maintained similar particle size, entrapment efficacy, and zeta potential, which was attributed to the high zeta potential which enhanced the colloidal stability and maintained electrostatic stabilization, additionally, the presence of PLX provided extra steric stabilization and prevented aggregation.[47]

Generally, mice are social organisms with a natural inclination to explore unfamiliar conspecifics. However, BTBR mice, along with other ASD mouse models, display a rather reserved demeanor with disinterest in social interaction, imitating some characteristics of human ASD. These mice frequently display repetitive behaviors and social communication deficits, which make them helpful for studying the mechanisms present in ASD. Studying social behavior is

significant not only to understand how cognitive and neural pathways function under normal circumstances, but also for interpreting how these mechanisms go wrong and then create uncharacteristic social behavior.[48–50] The three-chamber sociability and social novelty test is the most common method used to assess sociability and treatment effectiveness in ASD mouse models. This method analyzes the mouse's preference for a social stimulus (ie unfamiliar or novel mouse) or a non-social one (ie familiar mouse or empty cup).[51,52]

Automated quantifications in the three-chamber social tests encompass parameters such as total distance traveled, mean velocity, duration spent with the familiar mouse, empty cup or novel mouse, and duration spent in the center chamber at the nose-point or center-point, as well as behavioral patterns like self-grooming and sniffing. These factors give a complete overview of the social behavior and activity levels of the mice. The SI and SNI are calculated using Equation 1 and Equation 2, respectively. Although social communication is the major focus of this study, SI and SNI also offer insights into other attributes such as social memory and social motivation.[51] The greater the index value, the more social the mouse is, resembling the social phenotypes of WT mice. In essence, a greater SI value indicates the mouse's preference for the unfamiliar mouse over the empty cup and a greater SNI value indicates the mouse's preference for the unfamiliar or novel mouse over the familiar mouse. Using the three-chamber test therefore provides a consistent and dependable method to evaluate the social deficits present in ASD.

Figure 6A represents the heatmap for one of the C57 vehicle mice during the three-chamber social test where the test mouse displayed a preference inclined towards exploring the novel mouse over the empty cup and over the familiar mouse during the different test sessions. This response is normally observed in neurotypical individuals, due to their displayed curiosity and exploratory nature in unfamiliar environments. On the other hand, Figure 6B represents the heatmap for one of the BTBR vehicle mice during the three-chamber test. The BTBR mouse exhibited notable sociability impairment, as it was inclined to spend more time exploring the empty cup over the novel mouse and displayed no social preference towards the novel mouse compared to the familiar mouse, by spending more time exploring the familiar mouse. To extrapolate these findings, the exploration of non-social stimuli may bear a resemblance to the lack of interest in people and in creating relationships, which is a prominent behavioral characteristic of autistic individuals.[53] Social withdrawal is characteristic of ASD, as autistic individuals prefer to stay in environments that are deemed familiar with limited space for social interactions.[51]

Outcomes of the three-chamber sociability and social novelty tests confirmed low SI and SNI values for the BTBR vehicle group and higher values for the C57 control group, as anticipated. This, again, signifies notable sociability impairment in the BTBR vehicle mice, as opposed to the C57 control mice. BTBR mice treated with TQ-loaded nanovesicles exhibited increased SI and SNI values signifying improvement in social impairment, identified by their shift to explore the novel mouse over the empty cup or familiar mouse. BTBR mice receiving free TQ also exhibited increased SI and SNI values, however to a lesser degree, suggesting that nanovesicles may serve to enhance TQ delivery.[54]

These findings highlighted the potential of TQ-loaded nanovesicles as a promising therapeutic avenue for targeting social deficits in ASD compared to treatment with free TQ. The enhanced efficacy of the TQ-loaded nanovesicles may be attributed to their heightened bioavailability and targeted delivery, which facilitates the crossing of TQ across the BBB and continuous release at the target place of action. Although the effects of TQ-loaded nanovesicles on cognitive and social impairment and neural oxidative stress have not been previously studied in ASD, the therapeutic effects of TQ alone on social behavior and inflammation have been explored. Previous studies scrutinizing the neuroprotective potential of *Nigella sativa* confirmed the plant's ability to enhance cognition, memory, learning, and social behavior.[55–60] Together with a previous study conducted on the therapeutic effects of TQ on valproic acid-induced oxidative stress in rats that consequently exhibited ASD-like behavior,[61] this study's findings strengthen the postulation that TQ has the potential to modulate oxidative stress and thereby restored ASD-associated social deficits. The perceived enhancements in social behavior after administering TQ-loaded nanovesicles emphasize the role of oxidative stress in the pathophysiology of autism, showing that directing therapies to these pathways could be worthwhile in the treatment of autism.

Besides sociability impairment, ASD mouse models also exhibit repetitive behavior and increased anxiety. This encompasses extended periods of sniffing and self-grooming lasting up to 2 minutes as opposed to the typical 5 to 10 seconds observed in WT mice, repeated jumping and circling, restricted exploratory activity, impulse behavior, and an

abnormal sense of danger, to name a few.[62] Throughout the three-chamber and open field tests, prolonged periods of self-grooming and repetitive jumping and rotating in place were noted in the BTBR vehicle and BTBR carrier groups in contrast to the C57 control group. This observation aligns with the findings of previous studies that examined the duration of self-grooming in ASD mouse models.[63–65] Locomotor activity and exploratory behavior measured in the open field test are indicative of anxiety levels and danger perception in murine animal models. The parameters measured in the open field test include the total distance traveled, velocity, cumulative time spent in the center and periphery at the nose-point or center-point, and behavioral patterns like self-grooming and sniffing.

Figure 5A and B represent heatmaps of C57 and BTBR mice from the vehicle treatment group during the open field test, respectively. The BTBR mouse displayed increased locomotor activity, greater exploratory behavior, and traveled longer distances; this is characterized as hyperactivity which is a distinguishing feature of autistic mice. The BTBR mouse also spent more time in the center of the chamber compared to the periphery. This is often indicative of abnormal anxiety levels, in which autistic mice have cognitive impairment and lack proper danger perception resulting in impulsiveness and thereby, spending more time in the center which is considered a 'danger zone'. On the other hand, the C57 mouse was more likely to spend time hiding in the peripheral areas of the chamber as the WT mice typically gravitate towards the periphery perceiving it as a 'safe-zone';[66] this was notable in the C57 control mouse heatmap.

Although the pathogenesis of ASD is complex and multifaceted, oxidative stress and neuronal inflammation have been recognized to play a vital role in its pathogenesis. Therefore, therapies directed at such factors may offer promising treatment options,[1] with TQ as a great example, as it possesses notable antioxidant and anti-inflammatory properties. In this study, neuronal oxidative stress was assessed by measuring the levels of three oxidative stress markers, CAT, MDA, and GSH, in the cerebellum and hippocampus of the test mice. Oxidative stress poses oxidative damage to proteins, lipids, and DNA inside cells. It also prompts an array of reversible and irreversible biological and physiological damage in ASD. The connection between oxidative stress and ASD has lately been methodically reviewed[34] and elevated oxidative stress biomarkers have been linked with the severity of ASD.[35]

One key finding highlighted after biochemical analysis of the homogenized brain tissues was the marked reduction in the levels of the physiological antioxidative enzyme, CAT, and the antioxidant protein, GSH, which aligns with the diminished CAT and GSH activities described previously in ASD.[34] Nonetheless, upon treatment with the TQ-loaded nanovesicles, the levels of CAT and GSH were restored in the cerebellum and hippocampus of the BTBR mice. Similarly, aggravated levels of oxidative stress in ASD have been reported to deplete the stores of GSH in the body.[36] These results may be compared to the improvement in CAT and GSH levels in the BTBR mice that were treated with free TQ, and it is evident that this improvement is inferior to that observed with TQ-loaded nanovesicle treatment. Furthermore, elevated MDA levels have been identified as a distinctive sign of lipid peroxidation in ASD.[13] The untreated BTBR mice in this study initially had significantly increased levels of MDA in their brains. However, upon administration of TQ-loaded nanovesicles, the levels of MDA were considerably reduced in both the hippocampus and cerebellum, appearing almost similar to the levels of MDA normally present in the C57 control mice. Additionally, treatment with free TQ showed promising results in the hippocampus region, particularly. However, the best results in terms of MDA reduction were observed in the brains of the BTBR mice treated with TQ-loaded nanovesicles.

Conclusion

Owing to its wide range of pharmacological characteristics, TQ is increasingly being employed as a viable therapeutic agent in pharmaceutical research. This study particularly focused on the antioxidant of TQ as a potential therapeutic in mitigating brain damage caused by oxidative stress and thereby enhancing cognitive and behavioral patterns in autistic mice. To further improve TQ's bioavailability and guarantee targeted distribution to the afflicted brain areas, a nanovesicle-based drug delivery system was devised. Upon conducting behavioral assessments, it was revealed that TQ-loaded nanovesicles enhanced sociability and social novelty preference, modulated hyperactivity, and restored abnormal anxiety in the BTBR mice. After performing biochemical analysis, it was shown that TQ-loaded nanovesicles restored the levels of CAT and GSH in both the hippocampus and cerebellum. TQ-loaded nanovesicles also proved to diminish MDA levels in the cerebellum and the hippocampus, which are typically high in BTBR mice. These findings

strongly suggest that TQ-loaded nanovesicles hold great potential for modulating cognitive impairment in individuals with ASD.

Author Contributions

All authors made a significant contribution to the work reported, whether that is in the conception, study design, execution, acquisition of data, analysis and interpretation, or all these areas; took part in drafting, revising or critically reviewing the article; gave final approval of the version to be published; have agreed on the journal to which the article has been submitted; and agree to be accountable for all aspects of the work".

Funding

The Office of Graduate Studies and Research of UAE University is thanked for the support provided to BS with funds (12M099, 12R207, 12M182). NE acknowledges financial support from Abu Dhabi University's Office of Research and Sponsored Programs. Grant number: (19300837, 19300896).

Disclosure

The author(s) report no conflicts of interest in this work.

References

1. Usui N, Kobayashi H, Shimada S. Neuroinflammation and oxidative stress in the pathogenesis of autism spectrum disorder. *Int J Mol Sci*. 2023;24(6):5487. doi:10.3390/ijms24065487
2. Golden CE, Buxbaum JD, De Rubeis S. Disrupted circuits in mouse models of autism spectrum disorder and intellectual disability. *Curr Opin Neurobiol*. 2018;48:106–112. doi:10.1016/j.conb.2017.11.006
3. Katrin Sauer A, Stanton J E, Hans S, Grabrucker MA. Autism Spectrum Disorders: etiology and Pathology. In: Am G, editor. *Autism Spectrum Disorders*. Brisbane (AU): Exon Publications; 2021:1–5.
4. Kodak T, Bergmann S. Autism spectrum disorder: characteristics, associated behaviors, and early intervention. *Pediatr Clin N Am*. 2020;67(3):525–535. doi:10.1016/j.pcl.2020.02.007
5. van 't Hof M, Tisseur C, van Berckelear-Onnes I, et al. Age at autism spectrum disorder diagnosis: a systematic review and meta-analysis from 2012 to 2019. *Autism*. 2020;25(4):862–873. doi:10.1177/1362361320971107
6. Xiong J, Chen S, Pang N, et al. Neurological diseases with autism spectrum disorder: role of ASD risk genes. *Front Neurosci*. 2019;13:349. doi:10.3389/fnins.2019.00349
7. Christensen GM, Terrell ML, Pearce BD, et al. Exploring autism spectrum disorder (ASD) and attention deficit disorder (ADD/ADHD) in children exposed to polybrominated biphenyl. *Environ Epidemiol*. 2024;8(2):e304. doi:10.1097/EE9.0000000000000304
8. Forsyth L, McSorley M, Rydzewska E. All-cause and cause-specific mortality in people with autism spectrum disorder: a systematic review. *Res Autism Spectrum Disord*. 2023;105:102165. doi:10.1016/j.rasd.2023.102165
9. Leader G, Hogan A, Chen JL, et al. Age of autism spectrum disorder diagnosis and comorbidity in children and adolescents with autism spectrum disorder. *Develop Neurorehab*. 2022;25(1):29–37. doi:10.1080/17518423.2021.1917717
10. Aishworiya R, Valica T, Hagerman R, Restrepo B. An update on psychopharmacological treatment of autism spectrum disorder. *Neurotherapeutics*. 2022;19(1):248–262. doi:10.1007/s13311-022-01183-1
11. Pangrazzi L, Balasco L, Bozzi Y. Oxidative stress and immune system dysfunction in autism spectrum disorders. *Int J Mol Sci*. 2020;21(9):3293. doi:10.3390/ijms21093293
12. Ramaekers VT, Sequeira JM, Thöny B, Quadros EV. Oxidative stress, folate receptor autoimmunity, and CSF findings in severe infantile autism. *Autism Res Treat*. 2020;2020:9095284. doi:10.1155/2020/9095284
13. Uddin MN, Mondal T, Yao Y, Manley K, Lawrence DA. Oxidative stress and neuroimmune proteins in a mouse model of autism. *Cell Stress Chaperones*. 2023;28(2):201–217. doi:10.1007/s12192-023-01331-2
14. Eid EEM, Almaiman AA, Alshehade SA, et al. Characterization of thymoquinone-sulfobutylether-β-cyclodextrin inclusion complex for anticancer applications. *Molecules*. 2023;28(10):4096. doi:10.3390/molecules28104096
15. Pottoo FH, Ibrahim AM, Alammar A, et al. Thymoquinone: review of its potential in the treatment of neurological diseases. *Pharmaceuticals*. 2022;15(4):408. doi:10.3390/ph15040408
16. Almajali B, Al-Jamal HA, Taib WR, et al. Thymoquinone, as a novel therapeutic candidate of cancers. *Pharmaceuticals*. 2021;14(4):369. doi:10.3390/ph14040369
17. Mahmud NM, Paraoan L, Khaliddin N, Kamalden TA. Thymoquinone in ocular neurodegeneration: modulation of pathological mechanisms via multiple pathways. *Front Cell Neurosci*. 2022;16:786926. doi:10.3389/fncel.2022.786926
18. Isaev NK, Genrikhs EE, Stelmashook EV. Antioxidant thymoquinone and its potential in the treatment of neurological diseases. *Antioxidants*. 2023;12(2):433. doi:10.3390/antiox12020433
19. Goyal SN, Prajapati CP, Gore PR, et al. Therapeutic potential and pharmaceutical development of thymoquinone: a multitargeted molecule of natural origin. *Front Pharmacol*. 2017;8:656. doi:10.3389/fphar.2017.00656
20. Mittal KR, Pharasi N, Sarna B, et al. Nanotechnology-based drug delivery for the treatment of CNS disorders. *Transl Neurosci*. 2022;13(1):527–546. doi:10.1515/tnsci-2022-0258

21. Trummer F, Glatter O, Chemelli A. Inverse ISAsomes in bio-compatible oils-exploring formulations in squalane, triolein and olive oil. *Nanomaterials*. 2022;12(7):1133. doi:10.3390/nano12071133
22. Leu JSL, Teoh JJX, Ling ALQ, et al. Recent advances in the development of liquid crystalline nanoparticles as drug delivery systems. *Pharmaceutics*. 2023;15(5):1421. doi:10.3390/pharmaceutics15051421
23. Chen Y, Ma P, Gui S. Cubic and hexagonal liquid crystals as drug delivery systems. *Biomed Res Int*. 2014;2014:815981. doi:10.1155/2014/815981
24. Bakr MM, Shukr MH, ElMeshad AN. In situ hexosomal gel as a promising tool to ameliorate the transnasal brain delivery of vinpocetine: central composite optimization and in vivo biodistribution. *J Pharm Sci*. 2020;109(7):2213–2223. doi:10.1016/j.xphs.2020.03.030
25. Mehanna MM, Motawaa AM, Samaha MW. Tadalafil inclusion in microporous silica as effective dissolution enhancer: optimization of loading procedure and molecular state characterization. *J Pharm Sci*. 2011;100(5):1805–1818. doi:10.1002/jps.22420
26. Kulkarni P, Rawtani D. Application of Box-behnken design in the preparation, optimization, and in vitro evaluation of self-assembly-based tamoxifen- and doxorubicin-loaded and dual drug-loaded niosomes for combinatorial breast cancer treatment. *J Pharm Sci*. 2019;108 (8):2643–2653. doi:10.1016/j.xphs.2019.03.020
27. Rodrigues L, Kyriakos K, Schneider F, et al. Characterization of lipid-based hexosomes as versatile vaccine carriers. *Mol Pharm*. 2016;13 (11):3945–3954. doi:10.1021/acs.molpharmaceut.6b00716
28. Wang J, Guo F, Ma M, Mingzhu L, Tan F, Li N. Nanovesicular system containing tretinoin for dermal targeting delivery and rosacea treatment: a comparison of hexosomes, glycerosomes and ethosomes. *RSC Adv*. 2014;4:45458–66.
29. Xiao XY, Zhu YX, Bu JY, Li GW, Zhou JH, Zhou SP. Evaluation of neuroprotective effect of thymoquinone nanoformulation in the rodent cerebral ischemia-reperfusion model. *Biomed Res Int*. 2016;2016:2571060. doi:10.1155/2016/2571060
30. Elgindy NA, Mehanna MM, Mohyeldin SM. Self-assembled nano-architecture liquid crystalline particles as a promising carrier for progesterone transdermal delivery. *Int J Pharm*. 2016;501(1–2):167–179. doi:10.1016/j.ijpharm.2016.01.049
31. Fahelelbom KMS, Al-Tabakha MMM, Eissa NAM, Obaid DEE, Sayed S. Development and validation of an RP-HPLC analytical method for determination of lisinopril in full and split tablets. *Res J Pharm Technol*. 2020;13(6):2647. doi:10.5958/0974-360X.2020.00470.9
32. Zaki RM, Alkharashi LA, Sarhan OM, Almurshedi AS, Aldosari BN, Said M. Box Behnken optimization of cubosomes for enhancing the anticancer activity of metformin: design, characterization, and in-vitro cell proliferation assay on MDA-MB-231 breast and LOVO colon cancer cell lines. *Int J Pharm X*. 2023;6:100208. doi:10.1016/j.ijpx.2023.100208
33. Hanafy NAN, Abdelbadea RH, Abdelaziz AE, Mazyed EA. Formulation and optimization of folate-bovine serum albumin-coated ethoniosomes of pterostilbene as a targeted drug delivery system for lung cancer: in vitro and in vivo demonstrations. *Cancer Nanotechnol*. 2023;14(1):49. doi:10.1186/s12645-023-00197-4
34. Bjørklund G, Meguid NA, El-bana MA, et al. Oxidative stress in autism spectrum disorder. *Mol Neurobiol*. 2020;57(5):2314–2332. doi:10.1007/s12035-019-01742-2
35. Ghezzo A, Visconti P, Abruzzo PM, et al. Oxidative stress and erythrocyte membrane alterations in children with autism: correlation with clinical features. *PLoS One*. 2013;8(6):e66418. doi:10.1371/journal.pone.0066418
36. Liu X, Lin J, Zhang H, et al. Oxidative stress in autism spectrum disorder-current progress of mechanisms and biomarkers. *Front Psychiatry*. 2022;13:813304. doi:10.3389/fpsyt.2022.813304
37. Rein B, Ma K, Yan Z. A standardized social preference protocol for measuring social deficits in mouse models of autism. *Nat Protoc*. 2020;15 (10):3464–3477. doi:10.1038/s41596-020-0382-9
38. Jabarin R, Netser S, Wagner S. Beyond the three-chamber test: toward a multimodal and objective assessment of social behavior in rodents. *Mol Autism*. 2022;13(1):41. doi:10.1186/s13229-022-00521-6
39. Mohammad Y, Prentice RN, Boyd BJ, Rizwan SB. Comparison of cubosomes and hexosomes for the delivery of phenytoin to the brain. *J Colloid Interface Sci*. 2022;605:146–154. doi:10.1016/j.jcis.2021.07.070
40. Gupta N, Jain S, Jain V, Development RG. Characterization and evaluation of cubosomes loaded smart gel for the treatment of osteomyelitis using 32 factorial design. *INDIAN J PHARM EDUC RES*. 2023;57:695–702. doi:10.5530/ijper.57.3.84
41. Gupta T, Kenjale P, Pokharkar V. QbD-based optimization of raloxifene-loaded cubosomal formulation for transdermal delivery: ex vivo permeability and in vivo pharmacokinetic studies. *Drug Deliv Transl Res*. 2022;12(12):2979–2992. doi:10.1007/s13346-022-01162-1
42. Badie H, Abbas H. Novel small self-assembled resveratrol-bearing cubosomes and hexosomes: preparation, characterization, and ex vivo permeation. *Drug Dev Ind Pharm*. 2018;44(12):2013–2025. doi:10.1080/03639045.2018.1508220
43. Abreu AS, Castanheira EM, Queiroz MJ, Ferreira PM, Vale-Silva LA, Pinto E. Nanoliposomes for encapsulation and delivery of the potential antitumoral methyl 6-methoxy-3-(4-methoxyphenyl)-1H-indole-2-carboxylate. *Nanoscale Res Lett*. 2011;6(1):482. doi:10.1186/1556-276X-6-482
44. Mehanna MM, Sarieddine R, Alwattar JK, Chouaib R, Gali-Muhtasib H. Anticancer activity of thymoquinone cubic phase nanoparticles against human breast cancer: formulation, cytotoxicity and subcellular localization. *Int J Nanomed*. 2020;15:9557–9570. doi:10.2147/IJN.S263797
45. Swarnakar NK, Thanki K, Jain S. Bicontinuous cubic liquid crystalline nanoparticles for oral delivery of Doxorubicin: implications on bioavailability, therapeutic efficacy, and cardiotoxicity. *Pharm Res*. 2014;31(5):1219–1238. doi:10.1007/s11095-013-1244-8
46. Rizwan SB, Hanley T, Boyd BJ, Rades T, Hook S. Liquid crystalline systems of phytantriol and glyceryl monooleate containing a hydrophilic protein: characterisation, swelling and release kinetics. *J Pharm Sci*. 2009;98(11):4191–4204. doi:10.1002/jps.21724
47. Abdel-Bar HM, Khater SE, Ghorab DM and Al-mahallawi AM. (2020). Hexosomes as Efficient Platforms for Possible Fluoxetine Hydrochloride Repurposing with Improved Cytotoxicity against HepG2 CellsHexosomes as Efficient Platforms for Possible Fluoxetine Hydrochloride Repurposing with Improved Cytotoxicity against HepG2 Cells. *ACS Omega*. 5(41):26697–26709. doi:10.1021/acsomega.0c0356910.1021/acsomega.0c03569.s001
48. Ferretti V, Papaleo F. Understanding others: emotion recognition in humans and other animals. *Genes Brain Behav*. 2018;18(1):e12544.
49. Ferretti V, Maltese F, Contarini G, Chini B, Grinevich V, Papaleo F. Oxytocin signaling in the central amygdala modulates emotion discrimination in mice. *Curr Biol*. 2019;29(12). doi:10.1016/j.cub.2019.04.070
50. Bicks LK, Koike H, Akbarian S, Morishita H. Prefrontal cortex and social cognition in mouse and man. *Front Psychol*. 2015;6:1805. doi:10.3389/fpsyg.2015.01805
51. Kaidanovich-Beilin O, Lipina T, Vukobradovic I, Roder J, Woodgett JR. Assessment of social interaction behaviors. *J Vis Exp*. 2011;25(48):2473.
52. Yang M, Silverman JL, Crawley JN. Automated three-chambered social approach task for mice. *Curr Protoc Neurosci*. 2011. doi:10.1002/0471142301.ns0826s56

53. Davidson C, O'Hare A, Mactaggart F, et al. Social relationship difficulties in autism and reactive attachment disorder: improving diagnostic validity through structured assessment. *Res Dev Disabil*. 2015;40:63–72. doi:10.1016/j.ridd.2015.01.007
54. Ellegood J, Babineau BA, Henkelman RM, Lerch JP, Crawley JN. Neuroanatomical analysis of the BTBR mouse model of autism using magnetic resonance imaging and diffusion tensor imaging. *Neuroimage*. 2013;70:288–300. doi:10.1016/j.neuroimage.2012.12.029
55. Cheema MAR, Nawaz S, Gul S, et al. Neurochemical and behavioral effects of Nigella sativa and Olea europaea oil in rats. *Nutr Neurosci*. 2018;21(3):185–194. doi:10.1080/1028415X.2016.1257417
56. Ebrahimi SS, Oryan S, Izadpanah E, Hassanzadeh K. Thymoquinone exerts neuroprotective effect in animal model of Parkinson's disease. *Toxicol Lett*. 2017;276:108–114. doi:10.1016/j.toxlet.2017.05.018
57. Hosseini M, Zakeri S, Khoshdast S, et al. The effects of Nigella sativa hydro-alcoholic extract and thymoquinone on lipopolysaccharide - induced depression like behavior in rats. *J Pharm Bioallied Sci*. 2012;4(3):219–225. doi:10.4103/0975-7406.99052
58. Kadil Y, Tabyaoui I, Badre L, Jouti NT, Filali H. Evaluation of the antidepressant-like effect of chronic administration of nigella fixed oil versus fluoxetine in rats. *CNS Neurol Disord Drug Targets*. 2022;21(6):533–539. doi:10.2174/1871527320666211201160001
59. Lotfi M, Kazemi S, Ebrahimpour A, et al. Thymoquinone improved nonylphenol-induced memory deficit and neurotoxicity through its antioxidant and neuroprotective effects. *Mol Neurobiol*. 2022;59(6):3600–3616. doi:10.1007/s12035-022-02807-5
60. Samad N, Manzoor N, Muneer Z, Bhatti SA, Imran I. Reserpine-induced altered neuro-behavioral, biochemical and histopathological assessments prevent by enhanced antioxidant defence system of thymoquinone in mice. *Metab Brain Dis*. 2021;36(8):2535–2552. doi:10.1007/s11011-021-00789-2
61. Esmerce B, Aydin B, Tunçak S, Goren B. Effects of thymoquinone on valproic acid-induced oxidative stress in perinatal rat brain. *Anatolian J Botany*. 2023;7(1):76–81. doi:10.30616/ajb.1254803
62. Silverman JL, Yang M, Lord C, Crawley JN. Behavioural phenotyping assays for mouse models of autism. *Nat Rev Neurosci*. 2010;11(7):490–502. doi:10.1038/nrn2851
63. Hirsch MM, Deckmann I, Fontes-Dutra M, et al. Behavioral alterations in autism model induced by valproic acid and translational analysis of circulating microRNA. *Food Chem Toxicol*. 2018;115:336–343. doi:10.1016/j.fct.2018.02.061
64. Pearson BL, Pobbe RL, Defensor EB, et al. Motor and cognitive stereotypies in the BTBR T+tf/J mouse model of autism. *Genes Brain Behav*. 2011;10(2):228–235. doi:10.1111/j.1601-183X.2010.00659.x
65. Reynolds S, Urruela M, Devine DP. Effects of environmental enrichment on repetitive behaviors in the BTBR T+tf/J mouse model of autism. *Autism Res*. 2013;6(5):337–343. doi:10.1002/aur.1298
66. Simmons DH, Titley HK, Hansel C, Mason P. Behavioral tests for mouse models of autism: an argument for the inclusion of cerebellum-controlled motor behaviors. *Neuroscience*. 2021;462:303–319. doi:10.1016/j.neuroscience.2020.05.010